

Formation of nanocrystalline GeSn thin film on Si substrate by sputtering and rapid thermal annealing



H. Mahmodi ^a, M.R. Hashim ^{b,*}, U. Hashim ^c

^a Nano-Optoelectronics Research Laboratory, School of Physics, Universiti Sains Malaysia, 11800, USM, Pulau, Penang, Malaysia

^b Institute of Nano Optoelectronics Research and Technology (INOR), Universiti Sains Malaysia, 11800, USM, Pulau, Penang, Malaysia

^c Institute of Nano Electronic Engineering (INEE), University Malaysia Perlis (UniMAP), Kangar, Malaysia

ARTICLE INFO

Article history:

Received 15 August 2016

Accepted 19 August 2016

Available online 21 August 2016

Keywords:

Thin films

Nanocrystalline materials

Germanium-tin

Sputtering

Raman spectroscopy

HR-XRD

ABSTRACT

Nanocrystalline $\text{Ge}_{1-x}\text{Sn}_x$ thin films have been formed after rapid thermal annealing of sputtered GeSn layers. The alloy films were deposited onto the Silicon (100) substrate via low cost radio frequency magnetron sputtering. Then, the films were annealed by rapid thermal annealing at 350 °C, 400 °C, and 450 °C for 10 s. The morphological, structural, and optical properties of the layers were investigated with field emission scanning electron microscopy (FESEM), Energy-dispersive X-ray spectroscopy (EDX), Raman spectroscopy, and high-resolution X-ray diffraction (HR-XRD). The Raman analysis showed that the only observed phonon mode is attributed to Ge-Ge vibrations. Raman phonon intensities of GeSn thin films were enhanced with increasing the annealing temperature. The results clearly revealed that by increasing the annealing temperature the crystalline quality of the films were improved. The XRD measurements revealed the nanocrystalline phase formation in the annealed films with (111) preferred orientation. The results showed the potentiality of using the sputtering technique and rapid thermal anneal to produce crystalline GeSn layer.

© 2016 Elsevier Ltd. All rights reserved.

1. Introduction

$\text{Ge}_{1-x}\text{Sn}_x$ semiconductor alloy has received many interests in the last decade due to its potential major impact on microelectronic and photonic applications [1,2]. Fabrication of GeSn laser [3], GeSn light emitting diodes (LEDs) [4], p-GeSn/n-Ge diodes [5], GeSn photoconductors on Si [6] and sputtered GeSn p-i-n photodetectors on Ge [7] are the most important progress in this field. In addition, a wide range of Sn composition $0.025 < x < 0.19$ have been used for device fabrication [2,8–10]. One of the major driving force in attracting the interests is the incorporation of Sn in Ge, which convert the host from indirect to direct bandgap material. Hence, more efficient devices can be built from this material. However, the epitaxial growth and synthesis of $\text{Ge}_{1-x}\text{Sn}_x$ alloy is very challenging. First, Sn tends to segregate to the thin film surface [11]. Secondly, the equilibrium solid solubility of Sn in Germanium is rather low ($x < 0.01$) [12]. Finally, there is a large lattice mismatch (14.7%) between α -Sn and Ge. In addition, the lattice mismatch for a $\text{Ge}_{1-x}\text{Sn}_x$ alloy on Si (100) substrate is large (4.2–19%), which makes it hard to grow coherent epitaxial layer [13].

* Corresponding author.

E-mail address: roslan@usm.my (M.R. Hashim).

Despite these difficulties, this alloy can be grown in non-equilibrium growth systems like molecular beam epitaxy [14], chemical vapor deposition [15], pulsed laser deposition [16], solid phase crystallization [17] and sputtering [7]. Among deposition methods, magnetron sputtering is a suitable and low-cost technique for growing GeSn alloy films. Sputtering techniques allow us to easily control the deposition parameters, such as gas flow, substrate temperature, sputtering power, alloy composition, and deposition time [18].

Sputtered GeSn thin films at room temperature (RT) and lower elevated temperature are usually amorphous. This is due to the low surface mobility of adatoms at low temperature growth [19], which tends to induce additional point defect levels. Therefore, the levels of defects and lattice disorder in amorphous films need to be reduced by post-deposition annealing [20]. However, the morphological, structural and optical characteristics of the deposited GeSn alloys may also change in a subsequent thermal treatment. Nano crystalline and polycrystalline are the typical structures that formed during post deposition annealing.

This study reports on the formation of GeSn nanocrystalline layer on Si substrate upon rapid thermal annealing (RTA). GeSn thin films are co-sputtered simultaneously from high purity Ge and Sn targets onto a Si substrate at elevated substrate temperature. Then, some samples were subjected to the RTA at 350 °C, 400 °C, and 450 °C for 10 s. The results showed the effect of heat treatment on morphology, structural and optical properties of the co-sputtered GeSn thin films on Si substrates. The higher annealing temperature led to improved crystalline quality and optical characteristics of the co-sputtered GeSn layers.

2. Experimental procedure

Previously to growth, n-type Si (100) substrates were cleaned using RCA cleaning method. $\text{Ge}_{1-x}\text{Sn}_x$ alloys were deposited in a R.F. Magnetron sputtering system (Edwards A500, UK) on Si substrates with a base pressure of 1.20×10^{-5} mbar and Ar of high purity (99.999%). The thin film was deposited at substrate temperature of 140 °C. Both Ge (99.999%) and Sn (99.999%) targets have a diameter of 10 cm, and were set at a distance of 10 cm from the substrate. The magnetrons are located in planar configuration. The targets were co-sputtered for 30 min under RF sputtering power of 100 W for Ge and 15 W for Sn. After sputtering, some thin films were subjected to RTA at 350 °C, 400 °C, and 450 °C for 10 s in N₂ ambient. In a typical experiment, the as-sputtered sample was cut into pieces, and one of them was used as a reference of the as-sputtered sample.

Field emission scanning electron microscopy (FESEM) (model FEI-Nova NanoSEM 450) was utilized to analyze the surface morphology of thin films. Energy-dispersive X-ray spectroscopy (EDX) is utilized to identify the elements present in the samples at 10 KV. Raman spectroscopy was performed using a Jobin-Yvon (HR800UV) spectrometer to characterize the local atomic arrangements of the structures where the samples were excited at room temperature with an argon ion laser (514.5 nm, 20 mW). A high-resolution X-ray diffractometer (HR-XRD) system (X'Pert3040) devoted for the crystallographic investigation of the samples.

3. Results and discussion

The FESEM micrograph of an as-sputtered GeSn sample (Fig. 1(a)) showed coalesced small grains and a densely packed morphology. The FESEM images of the annealed GeSn samples at various temperatures are shown in Fig. 1(b–d). The sample annealed at 350 °C has almost the same morphology as the as-sputtered one. Significant difference were observed in the morphology of the samples c and d, which annealed at higher temperature of 400 °C and 450 °C. In these samples, it can be seen that the small clusters are joined to each other and made larger feathers, as shown in Fig. 1(c). In fact, the previously smooth film has clearly coalesced into clusters. However, in Fig. 1(d), pores are observed for the film annealed at the higher annealing temperature of 450 °C. The appearance of pores on the film surface suggested that is due to the Sn surface segregation at this higher annealing temperature. There are no signs of Sn surface segregation on the surface of the as-sputtered sample. Fig. 2 shows the cross sectional FESEM images of the thin films. The as-sputtered sample layer thickness is about 240 nm, as shown in Fig. 2(a). The alloy films annealed at higher temperature of 400 °C and 450 °C show some features when compared with that of the other samples. These results indicate the significant changes in the surface morphology of GeSn films upon rapid thermal annealing.

Fig. 3 shows the spectra image obtained by typical EDX of the as-sputtered sample. Four basic peaks were formed at 0.52, 1.18, 1.73, and 3.44 keV, which match to the spectral lines of O, Ge, Si, and Sn, respectively. Si originated from the substrate, and O is most likely due to the surface oxidation of GeSn film. The Ge and Sn concentrations of all of the samples are listed in Table 1. Sn atomic concentration of the as-sputtered sample is 12%, while it's concentration for the annealed samples at 350 °C, 400 °C and 450 °C continuously decreased to 7%, 3%, and 1.6%, respectively, after selective etching away of segregated Sn to the films surface [21]. A sharp and intense Ge peak is related to the sputtered GeSn thin film. A reduction of the Sn content in the annealed samples is attributed to the surface segregation, as evident in the FESEM image of the samples annealed at higher temperature. It is clear that the RTA affected on the composition of the sputtered films.

Fig. 4 shows the Raman spectra of all samples taken at room temperature. The spectrum from bulk n-Ge (100) wafer was also included in the inset of Fig. 4. The Ge spectrum revealed a strong Ge longitudinal-optical (LO) phonon peak at $\sim 301.03 \text{ cm}^{-1}$ [22]. The phonon peak position, intensity, full width at half-maximum (FWHM), and peak shift for all samples are summarized in Table 2.

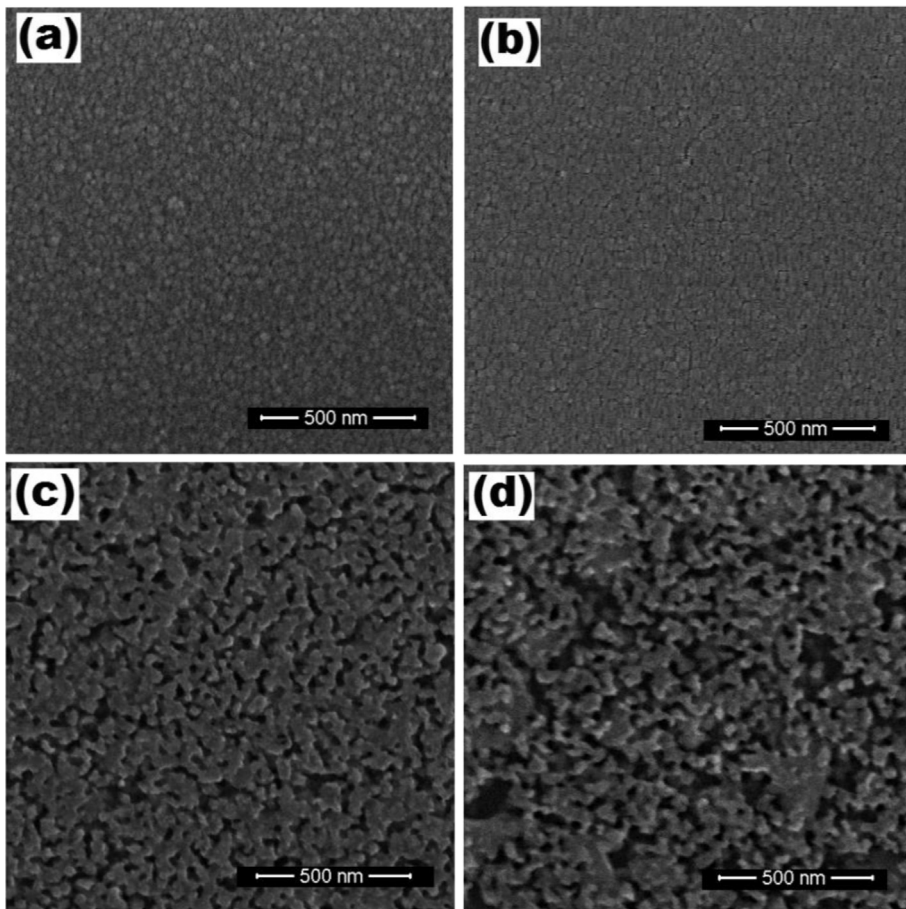


Fig. 1. FESEM images of (a) the as-sputtered and rapid thermal annealed samples at (b) 350 °C, (c) 400 °C and (d) 450 °C.

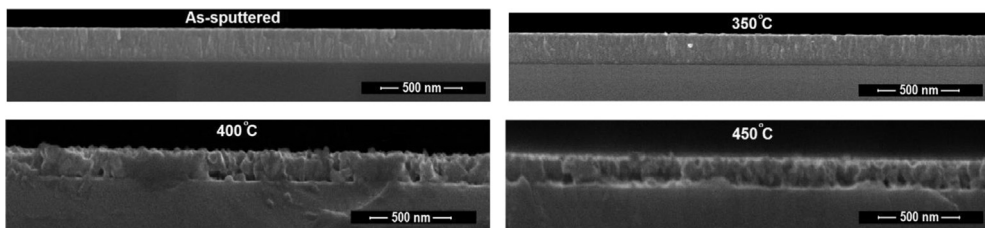


Fig. 2. Cross-sectional FESEM images of the as-sputtered and annealed thin films.

Raman frequency modes corresponding to Ge-Ge, Ge-Sn, and Sn-Sn modes are expected to be observed in GeSn alloy films. The observed peak at 520.1 cm^{-1} is belonged to Si substrate. Given that the grown samples are Ge-rich, the observed peak can be definitely indexed to Ge-Ge vibrations. The Ge-Sn modes are not found in our spectra. Since the laser wavelength of 532 nm, used in this study, is far from the resonance condition with the $E_1 - E_1 + \Delta_1$ optical transitions, as suggested by D'Costa et al. [23,24]. The Ge-Sn bond is observed when the layer is excited by a laser with wavelengths of 633 nm [25,26] and 647.1 nm [24]. Sn-Sn peaks could not be found in the Raman spectra due to the small amount of Sn and peak broadening.

As can be seen in Fig. 4, the intensity of Ge-Ge peak increased after post deposition annealing. The samples annealed at higher temperature of 400 °C and 450 °C exhibit highest phonon peak intensity than that of the as-sputtered one. The phonon peak intensity of the corresponding peaks are almost 2.5 times higher than that of the as-sputtered one, which shows higher interactions with incident photons. These features show an improvement in the crystallite structure of GeSn film upon heat treatment.

The peak position of the Ge-Ge mode shifted during the rapid thermal annealing. Note that it shifts to higher frequency with increasing the annealing temperature. In semiconductor alloys, the Raman frequency shift is known to be affected

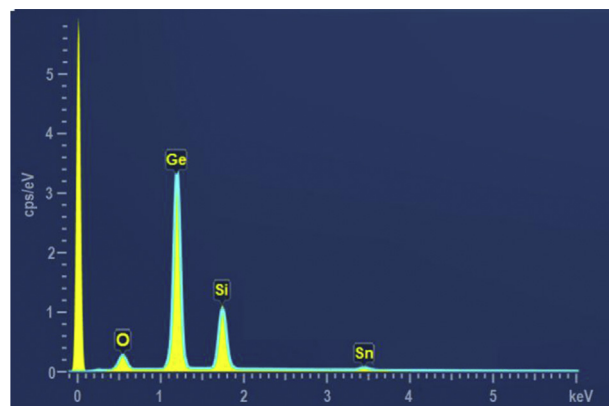


Fig. 3. The typical EDX spectra of the $\text{Ge}_{1-x}\text{Sn}_x$ thin film, which belongs to the as-sputtered sample.

Table 1

The Ge and Sn atomic concentration of the as-sputtered sample and annealed samples at various temperature ($\text{Ge}_{1-x}\text{Sn}_x$).

Samples	Atomic concentration (%)	
	Ge	Sn
As-sputtered	0.88	12
350 °C	0.93	7
400 °C	0.97	3
450 °C	0.98	1.6

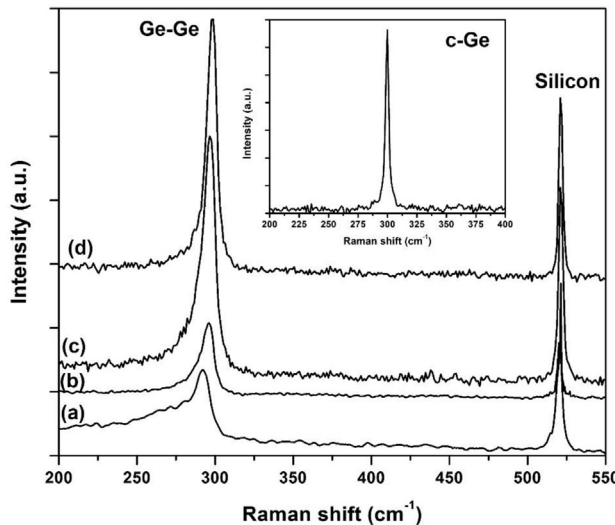


Fig. 4. The Raman spectra of (a) as-sputtered sample and annealed samples at (b) 350 °C, (c) 400 °C, and (d) 450 °C. The inset shows the spectrum from a bulk n-Ge (100) wafer.

Table 2

The details of the Ge-Ge mode of Raman spectra for as-sputtered and annealed GeSn samples. The frequency shift value is compared to the as-sputtered sample.

Samples	Ge-Ge (cm^{-1})	Peak intensity (a.u.)	FWHM (cm^{-1})	Raman shift (cm^{-1})	W_L/W_R
C-Ge	301.03	3218.00	3.88	—	1
A (As-sputtered)	292.17	974.22	16.12	—	—
B (350 °C)	295.78	1230.25	15.47	3.60	2.01
C (400 °C)	296.60	2350.00	13.86	4.43	1.82
D (450 °C)	298.82	2318.50	9.03	6.64	1.74

mostly due to the compositional variation and strain [27]. The highest annealed sample at 450 °C has the largest shift, which is 6.64 cm⁻¹, compared to the as-grown sample. Meanwhile, the Ge-Ge peaks of all samples were left-shifted in comparison with bulk Ge (301.03 cm⁻¹).

The FWHM of the Ge-Ge peak began to reduce by increasing the annealing temperature. As shown in Table 2, the FWHM of the sample D is 9.03 cm⁻¹, is smaller than that of the as-grown, which is 16.12 cm⁻¹. This feature indicates an enhancement in the crystalline quality of annealed samples at higher temperature compared to as-grown one.

A broadening and asymmetry can be observed in the entire Ge-Ge curves. This feature previously has been observed in the Ge-Ge phonon peak in the GeSn alloy [28]. Broadening of the Ge-Ge peak, which is more obvious in the as-grown and 350 °C annealed samples, is attributed to compositional fluctuations and local disorder [29,30]. However, this feature was reduced in the samples C and D by increasing the annealing temperature, which indicates an enhancement in the crystalline structure.

Due to the asymmetry of the Ge-Ge Raman peaks, the half width at half maximum (HWHM) were obtained, as mentioned in Ref. [31]. The Raman spectra show that the HWHM on the left low-energy side (W_L) is obviously larger than the right high-energy side (W_R). As given in Table 2, the W_L/W_R value was gradually reduced by increasing the annealing temperature, which means decreasing the asymmetry, as well as indicating the increase in crystalline quality. As reported in Ref. [31], the ratio of W_L/W_R has a direct relationship with Sn concentration, as observed in this study. Here, as the Sn concentration was reduced there was a decrease in the W_L/W_R value. It is suggested that the observed asymmetry and shifted in Ge-Ge peak is due to the Sn addition to the Ge. Thus, regarding the existence of asymmetry over the low frequency side of the spectra and considering the ratio of W_L/W_R , it is suggested the presence and formation of nanocrystalline GeSn upon heat treatment.

Fig. 5 shows the HR-XRD patterns of the annealed GeSn layers. The spectrum of the as-sputtered sample was also provided for comparison. The sharpest peak observed at $2\theta = 69.32^\circ$ is attributed to the Si (400) substrate. The XRD measurement of as-sputtered and annealed co-sputtered GeSn layers at various annealing temperatures are given in Table 3.

The pattern of the as-sputtered sample shows a low intensity peak at $2\theta = 26.37^\circ$, which are between those 2θ angles for a-Sn (111) and c-Ge (111), 23.7°~27.3°. This peak is attributed to the cubic GeSn (111) structure [32], which shows the evidence of initial crystallization. The observation of this peak for the as-deposited sample was expected as the substrate heating was used during deposition. This cubic peak became pronounced as the annealing temperature was raised, due to the improvement in crystalline quality of GeSn films. The (111) diffraction pattern has shifted to higher angle for the annealed samples, as compared to the as-sputtered sample. The peaks position for the annealed samples at temperature of 350 °C, 400 °C and 450 °C are observed at $2\theta = 26.95^\circ$, 27.12°, and 27.20°, respectively.

The average crystallite size was estimated from the FWHM by Scherrer's formula [33]:

$$D = \frac{0.9\lambda}{\beta \cos \theta} \quad (1)$$

where D is the crystallite size, β is the broadening of the diffraction line measured at half of its maximum intensity in radian, λ is the wavelength of the X-Ray used (1.54 Å) and θ is the diffraction angle. The largest crystallite size was obtained for the sample annealed at 450 °C, which is 27.86 nm. For the as-sputtered sample, the crystallite size is 1.46 nm. It can be seen that the crystallite size is increasing by raising the annealing temperature. The creation of the large crystallite size is due to the high-temperature annealing, which leads to the high mobility of individual atoms over the crystallite surface [34]. The

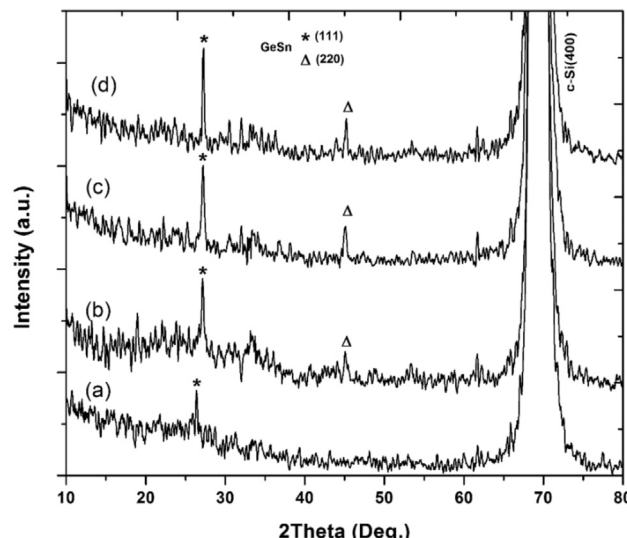


Fig. 5. HR-XRD spectra of (a) the as-sputtered GeSn thin films on the Si substrate and rapid thermal annealed films at (b) 350 °C, (c) 400 °C, and (d) 450 °C.

Table 3

The XRD data for the GeSn samples with different annealing temperatures.

Sample	Orientation	2θ (Deg.)	FWHM (Deg.)	Crystallite size (nm)	Sn composition (%)
As grown 350 °C	(111)	26.37	1.05	1.46	17
	(111)	26.95	1.20	7.09	7.9
	(220)	45.02	0.81	11.05	
400 °C	(111)	27.12	0.49	17.10	3.8
	(220)	45.12	0.50	17.86	
450 °C	(111)	27.20	0.30	27.86	1.9
	(220)	45.22	0.40	22.11	

improvement in the average crystallite size during annealing can be concluded from the reduced FWHM values of the layers diffraction peaks. Thus, the results demonstrate an improvement in the crystalline quality of GeSn layers because of the post deposition annealing. This is attributed to the mobility of atoms at different annealing temperatures [35].

Another diffraction pattern is observed just for the annealed samples at the orientation of (220), which are between those 2θ angles for a-Sn (220) and c-Ge (220), $39.2^\circ \sim 45.3^\circ$. This pattern is observed at $2\theta = 45.02^\circ$, $2\theta = 45.12^\circ$, and $2\theta = 45.22^\circ$ for the annealed samples at temperature of 350 °C, 400 °C and 450 °C, respectively. These small shifts to higher 2θ angle were observed by increasing the annealing temperature. It can be suggested that this is due to the Sn reduction in the films during annealing due to the Sn surface segregation. The 2θ shifts in (220) peak yield the same results.

The Sn concentration (atomic) in the GeSn films was estimated by Vegard's law on the basis of the lattice constant of GeSn, for the 2θ angle of (111) diffraction. The shift in (220) peaks yield the same results. For the binary compound $\text{Ge}_{1-x}\text{Sn}_x$ Vegard's law has the form [36]:

$$a(x) = a_{\text{Ge}}(1 - x) + a_{\text{Sn}}x + b_{\text{GeSn}}x(1 - x) \quad (2)$$

Where a is the lattice constant, x is the Sn concentration, and b is the bowing parameter of GeSn ($b = 0.041 \text{ \AA}$) [37]. As shown in Table 3, the estimated Sn compositions from XRD are 7.9%, 3.8%, 1.9% for the film annealed at the 350 °C, 400 °C, and 450 °C, respectively. The lower Sn concentration for the sample annealed at 450 °C indicates the less Sn dissolving in GeSn, as evident from the peak shifting to higher angle. This is in consistent with Raman results, which observed that the Ge-Ge phonon modes were shifted to higher frequency with decreasing the Sn concentration.

The grown GeSn films in this study were crystallized at low crystallization temperature of 350–450 °C, which is comparable to other rapid thermal annealing studies [21,38].

4. Conclusions

Nanocrystalline $\text{Ge}_{1-x}\text{Sn}_x$ thin films have been successfully grown on Si(100) substrate by RF magnetron sputtering after rapid thermal annealing. The Raman spectroscopy result shows an enhancement in the phonon intensities of annealed samples with increasing the annealing temperature, indicating the improvement in the GeSn crystalline quality. The XRD results indicated that upon rapid thermal annealing process, the crystalline phase of the material improved significantly with (111) preferred orientation. The layer annealed at 450 °C had the most intense peak and largest crystallite size (27.86 nm) compared to the layers annealed at lower temperatures. It was found that the higher annealing temperature significantly improved the crystalline quality of the sputtered GeSn layers, and enhanced the optical characteristics. The results showed the potentiality of using the sputtering technique and rapid thermal anneal to produce crystalline GeSn layer for photonic and light sensing device applications.

Acknowledgement

The support from grant 1001/PFIZIK/846072 and Universiti Sains Malaysia are gratefully acknowledged.

References

- [1] R. Soref, Mid-infrared photonics in silicon and germanium, *Nat. Phot.* 4 (2010) 495–497.
- [2] H. Wang, Y. Liu, M. Liu, Q. Zhang, C. Zhang, X. Ma, J. Zhang, Y. Hao, G. Han, Performance improvement in novel germanium–tin/germanium heterojunction-enhanced p-channel tunneling field-effect transistor, *Superlattices Microstruct.* 83 (2015) 401–410.
- [3] S. Wirths, R. Geiger, N. von den Driesch, G. Müssler, T. Stoica, S. Mantl, Z. Ikonik, M. Lüysberg, S. Chiussi, J.M. Hartmann, H. Sigg, J. Faist, D. Buca, D. Grützmacher, Lasing in direct-bandgap GeSn alloy grown on Si, *Nat. Phot.* 9 (2015) 88–92.
- [4] W. Du, Y. Zhou, S.A. Ghosh, A. Mosleh, B.R. Conley, A. Nazzal, R.A. Soref, G. Sun, J. Tolle, J. Margetis, H.A. Naseem, S.-Q. Yu, Room-temperature electroluminescence from $\text{Ge}/\text{Ge}_{1-x}\text{Sn}_x/\text{Ge}$ diodes on Si substrates, *Appl. Phys. Lett.* 104 (2014) 241110.
- [5] B. Baert, S. Gupta, F. Gencarelli, R. Loo, E. Simoen, N.D. Nguyen, Electrical characterization of p-GeSn/n-Ge diodes with interface traps under dc and ac regimes, *Solid State Electron.* 110 (2015) 65–70.
- [6] B.R. Conley, A. Mosleh, S.A. Ghosh, W. Du, R.A. Soref, G. Sun, J. Margetis, J. Tolle, H.A. Naseem, S.-Q. Yu, Temperature dependent spectral response and detectivity of GeSn photoconductors on silicon for short wave infrared detection, *Opt. Express* 22 (2014) 15639–15652.
- [7] J. Zheng, S. Wang, Z. Liu, H. Cong, C. Xue, C. Li, Y. Zuo, B. Cheng, Q. Wang, GeSn p-i-n photodetectors with GeSn layer grown by magnetron sputtering epitaxy, *Appl. Phys. Lett.* 108 (2016) 033503.

- [8] C. Chang, H. Li, S.H. Huang, H.H. Cheng, G. Sun, R.A. Soref, Sn-based Ge/Ge_{0.975}Sn_{0.025}/Ge p-i-n photodetector operated with back-side illumination, *Appl. Phys. Lett.* 108 (2016) 151101.
- [9] S. Kim, J. Gupta, N. Bhargava, M. Coppinger, J. Kolodzey, Current–voltage characteristics of GeSn/Ge heterojunction diodes grown by molecular beam epitaxy, *IEEE Electron Device Lett.* 34 (2013) 1217–1219.
- [10] Y. Liu, J. Yan, H. Wang, B. Cheng, G. Han, Strained germanium–tin (GeSn) P-Channel metal-oxide-semiconductor field-effect transistors featuring high effective hole mobility, *Int. J. Thermophys.* 36 (2015) 980–986.
- [11] P.R. Pukite, A. Harwit, S.S. Iyer, Molecular beam epitaxy of metastable, diamond structure Sn_xGe_{1-x} alloys, *Appl. Phys. Lett.* 54 (1989) 2142–2144.
- [12] C.D. Thurmond, F.A. Trumbore, M. Kowalchik, Germanium solidus curves, *J. Chem. Phys.* 25 (1956) 799–800.
- [13] W. Wang, S. Su, J. Zheng, G. Zhang, C. Xue, Y. Zuo, B. Cheng, Q. Wang, Flattening of low temperature epitaxial Ge_{1-x}Sn_x/Ge/Si(100) alloys via mass transport during post-growth annealing, *Appl. Surf. Sci.* 257 (2011) 4468–4471.
- [14] A.S. Nikolenko, V.V. Strelichuk, N.V. Safruk, S.B. Kryvyi, V.P. Kladko, O.S. Oberemok, L.V. Borkovska, Y.G. Sadofyev, Structural and optical studies of strain relaxation in Ge_{1-x}Sn_x layers grown on Ge/Si(001) by molecular beam epitaxy, *Thin Solid Films* 613 (2015) 68–74.
- [15] F. Gencarelli, Y. Shimura, A. Kumar, B. Vincent, A. Moussa, D. Vanhaeren, O. Richard, H. Bender, W. Vandervorst, M. Caymax, R. Loo, M. Heyns, Amorphous inclusions during Ge and GeSn epitaxial growth via chemical vapor deposition, *Thin Solid Films* 590 (2015) 163–169.
- [16] S. Stefanov, J.C. Conde, A. Benedetti, C. Serra, J. Werner, M. Oehme, J. Schulze, D. Buca, B. Holländer, S. Mantl, S. Chiussi, Silicon germanium tin alloys formed by pulsed laser induced epitaxy, *Appl. Phys. Lett.* 100 (2012) 204102.
- [17] O. Nakatsuka, K. Mochizuki, Y. Shimura, T. Yamaha, S. Zaima, Low temperature formation of Si_{1-x-y}Ge_xSn_y-on-insulator structures by using solid-phase mixing of Ge_{1-x}Sn_x/Si-on-insulator substrates, *Thin Solid Films* 520 (2012) 3288–3292.
- [18] A. Samavati, Z. Othaman, S.K. Ghoshal, F. Ahmadi, Self-assembled Ge/Si nanoislands: effect of argon flow and radio frequency power, *Phys. Scr.* 89 (2014) 025004.
- [19] R.R. Lieten, C. Fleischmann, S. Peters, N.M. Santos, L.M. Amorim, Y. Shimura, N. Uchida, T. Maeda, S. Nikitenko, T. Conard, J.-P. Locquet, K. Temst, A. Vantomme, Structural and Optical Properties of amorphous and crystalline GeSn layers on Si, *ECS J. Solid State Sci. Technol.* 3 (2014) 403–408.
- [20] R. Roucka, Y.Y. Fang, J. Kouvettakis, A.V.G. Chizmeshya, J. Menéndez, Thermal expansivity of Ge_{1-y}Sn_y alloys, *Phys. Rev. B* 81 (2010) 245214.
- [21] H. Li, J. Brouillet, A. Salas, X. Wang, J. Liu, Low temperature growth of high crystallinity GeSn on amorphous layers for advanced optoelectronics, *Opt. Mater. Express* 3 (2013) 1385–1396.
- [22] D.R. dos Santos, I.L. Torriani, Crystallite size determination in μc-Ge films by x-ray diffraction and Raman line profile analysis, *Solid State Commun.* 85 (1993) 307–310.
- [23] V.R. D'Costa, J. Tolle, C.D. Poweleit, J. Kouvettakis, J. Menéndez, Compositional dependence of Raman frequencies in ternary Ge_{1-x-y}Si_xSn_y alloys, *Phys. Rev. B* 76 (2007) 035211.
- [24] V.R. D'Costa, J. Tolle, R. Roucka, C.D. Poweleit, J. Kouvettakis, J. Menéndez, Raman scattering in Ge_{1-y}Sn_y alloys, *Solid State Commun.* 144 (2007) 240–244.
- [25] M. Oehme, D. Buca, K. Kostecki, S. Wirths, B. Holländer, E. Kasper, J. Schulze, Epitaxial growth of highly compressively strained GeSn alloys up to 12.5% Sn, *J. Cryst. Growth* 384 (2013) 71–76.
- [26] J.-H. Fournier-Lupien, S. Mukherjee, S. Wirths, E. Pippel, N. Hayazawa, G. Mussler, J.M. Hartmann, P. Desjardins, D. Buca, O. Moutanabbir, Strain and composition effects on Raman vibrational modes of silicon-germanium-tin ternary alloys, *Appl. Phys. Lett.* 103 (2013) 263103.
- [27] M.Z. Hossain, H.T. Johnson, Effects of composition, strain, and atomic disorder on optical phonon frequencies in Si_{1-x}Ge_x, *J. Appl. Phys.* 107 (2010) 1–6.
- [28] S. Stefanov, J.C. Conde, A. Benedetti, C. Serra, J. Werner, M. Oehme, J. Schulze, S. Chiussi, Laser assisted formation of binary and ternary Ge/Si/Sn alloys, *Thin Solid Films* 520 (2012) 3262–3265.
- [29] S.F. Li, M.R. Bauer, J. Menéndez, J. Kouvettakis, Scaling law for the compositional dependence of Raman frequencies in SnGe and GeSi alloys, *Appl. Phys. Lett.* 84 (2004) 867–869.
- [30] M. Rojas-López, H. Navarro-Contreras, P. Desjardins, O. Gurdal, N. Taylor, J.R.A. Carlsson, J.E. Greene, Raman scattering from fully strained Ge_{1-x}Sn_x(x≤0.22) alloys grown on Ge(001)2×1 by low-temperature molecular beam epitaxy, *J. Appl. Phys.* 84 (1998) 2219–2223.
- [31] S. Su, W. Wang, B. Cheng, W. Hu, G. Zhang, C. Xue, Y. Zuo, Q. Wang, The contributions of composition and strain to the phonon shift in Ge_{1-x}Sn_x alloys, *Solid State Commun.* 151 (2011) 647–650.
- [32] F. Hirofumi, M. Hiroaki, N. Toshio, I. Takeshi, O. Yukio, Structural changes of amorphous Ge_{1-x}Sn_x alloy films by annealing, *Jpn. J. Appl. Phys.* 25 (1986) 1312.
- [33] A. Ramadoss, K. Krishnamoorthy, S.J. Kim, Facile synthesis of hafnium oxide nanoparticles via precipitation method, *Mater. Lett.* 75 (2012) 215–217.
- [34] K. Yoichi, S. Takaaki, K. Shinji, Temperature dependence of mobility in silicon (100) inversion layers at low temperatures, *Surf. Sci.* 113 (1982) 218–222.
- [35] G. Galvagno, F. Roccaforte, A. Ruggiero, L. Calcagno, E. Zanetti, M. Saggio, F. Portuese, F. La Via, Temperature dependence of the c-axis drift mobility in 4H-SiC, *Microelectron. Eng.* 83 (2006) 45–47.
- [36] L. Vegard, Die Konstitution der Mischkristalle und die Raumfüllung der Atome, *Z. Phys.* 5 (1921) 17–26.
- [37] F. Gencarelli, B. Vincent, J. Demeulemeester, A. Vantomme, A. Moussa, A. Franquet, A. Kumar, H. Bender, J. Meerschaut, W. Vandervorst, R. Loo, M. Caymax, K. Temst, M. Heyns, Crystalline properties and strain relaxation mechanism of CVD grown GeSn, *ECS Trans.* 50 (2013) 875–883.
- [38] B.R. Conley, A. Mosleh, S.A. Ghetmiri, W. Du, G. Sun, R. Soref, J. Margitis, J. Tolle, H.A. Naseem, S.-Q. Yu, Stability of pseudomorphic and compressively strained Ge_{1-x}Sn_x thin films under rapid thermal annealing, *ECS Trans.* 64 (2014) 881–893.